Journal of Molecular Liquids 240 (2017) 329–339

Contents lists available at ScienceDirect

Journal of Molecular Liquids

journal homepage: www.elsevier.com/locate/molliq

Methyl orange removal from aqueous solution using goethite, chitosan beads and goethite impregnated with chitosan beads

Venkata Subbaiah Munagapati [a], Vijaya Yarramuthi [b], Dong-Su Kim [a,*]

[a] Department of Environmental Science and Engineering, Ewha Womans University, 11-1 Daehyun-Dong, Seodaemun-Gu, Seoul 120-750, Republic of Korea
[b] Department of Chemistry, Vikrama Simhapuri University, Nellore 524-003, Andhra Pradesh, India

ARTICLE INFO

Article history:
Received 20 March 2017
Received in revised form 26 April 2017
Accepted 22 May 2017
Available online 23 May 2017

Keywords:
Adsorption
Methyl orange
Isotherms
Kinetics
Thermodynamics
Temperature

ABSTRACT

The adsorption of methyl orange (MO) onto goethite (G), chitosan beads (CSB) and goethite impregnated with chitosan beads (GCSB) as a new and potential adsorbents have been studied. Batch adsorption studies were conducted to evaluate the effect of various parameters such as pH, contact time, initial dye concentration and temperature. The adsorbents are characterized by using Fourier Transform Infrared Spectroscopy (FTIR), Scanning Electron Microscopy (SEM) and Brunner-Emmet-Teller (BET) analysis, respectively. FTIR results revealed that hydroxyl, amine and carboxyl functional groups present on the surface of adsorbents. Experimental equilibrium data for adsorption of MO was analyzed by the Langmuir, Freundlich and Dubinin-Radushkevich models. The results showed that the best fit was achieved with the Langmuir isotherm equation with maximum adsorption capacities of 55, 73 and 84 mg/g for G, CSB and GCSB, respectively. The pseudo-first-order and pseudo-second-order model equations were used to analyze the kinetic data of the adsorption process and the data was fitted well with the pseudo-second-order kinetic model. The calculated thermodynamic parameters, namely ΔG^o, ΔH^o and ΔS^o showed that adsorption of MO was spontaneous and endothermic in the temperature range 298–338 K. Desorption experiments were carried out to explore the feasibility of regenerating the adsorbent and the adsorbed MO from G, CSB and GCSB were desorbed using 0.1 M NaOH with an efficiency of 91, 94 and 96%, respectively, recovery. Findings of the present study indicated that G, CSB and GCSB can be successfully used for removal of MO from aqueous solution.

1. Introduction

The removal of hazardous materials such as dyes, heavy metals and aromatic compounds from industrial effluents is of great environmental concern [1]. The extensive application of dye compounds in various industries such as textile, leather, paper, rubber, paint and plastics lead to discharges toxic colored effluent and contaminates surface and ground water. There are over 100,000 commercially available dyes and $>7 \times 10^5$ tones are produced annually. The presence of small amounts of dyes in water is highly visible and undesirable. Dyes are resistant to heat, chemical reagent and have the ability to generate cancer and mutagens. Presence of dyes in water creates serious impact for different aquatic organisms [2]. Therefore, their removal from wastewater before the dyes had entered into human bodies through water is of great demand. Azo dyes with high brightness in color due to the presence of azo (—N═N—) groups in cooperation with substituted aromatic structures have more toxicity to living organisms [3]. Methyl orange (MO), an anionic dye belongs to the azo group of dyes. MO has been widely used in textile, paper, plastics, rubber, cosmetics, printing, dye manufacturing and pharmaceutical industries [4]. The presence of azo group on MO and low biodegradability makes it an issue of concern for environmental science [5]. MO leads to health hazards such as vomiting, diarrhea, breathing and nausea. It is a weak acid base indicator with potential applicability as toxic and carcinogenic agent. Therefore, its removal and elimination from various aqueous wastes is required. There are various methods to treat dyes from contaminated water, such as adsorption [6], chemical oxidation [7], chemical reduction [8] photodegradation [9], electrochemical oxidation [10], coagulation-flocculation [11], biological treatment [12] and membrane separation [13]. Among these methods, adsorption process has been shown to be an effective technique with its efficiency, capacity, and applicability on a large scale to remove dyes as well as having the potential for regeneration, recovery, and recycling of adsorbents.

Iron oxides, a common constituent of soils, sediments, and aquifers, have high surface areas and are capable of adsorbing a significant quantity of dyes. Goethite, is a common oxy-hydroxide in natural environment and has the dia-spore structure which is based on hexagonal close packing and consists of a large amount of reactive surface hydroxyl sites, however it can be synthetically produced. Chitosan, β-(1-4) acetyl-D-glucosamine, is a linear biopolymer of glucosamine. It can be produced commercially by chemical deacetylation of chitin, a major

* Corresponding author.
E-mail address: dongsu@ewha.ac.kr (D.-S. Kim).

http://dx.doi.org/10.1016/j.molliq.2017.05.099
0167-7322/

component of the exoskeleton of crustaceans (such as lobster, crabs and shrimp) and cell walls of fungi and algae, therefore it is the second most abundant biological resource after cellulose. Chitosan has biological and chemical properties such as non-toxicity, high chemical reactivity, hydrophilicity, biocompatibility, biodegradability, chirality, chelation, anti-bacterial properties and adsorption properties [14]. The application of biopolymers such as chitin and chitosan is one of the emerging adsorption methods for the removal of dyes and metal ions due to the presence of amino (—NH_2) and hydroxyl (—OH) groups, which can serve as the active sites even at low concentrations [15]. In recent years, various types of chitosan based adsorbents such as α-Fe_2O_3 impregnated chitosan beads [16], magnetic nanoparticles impregnated chitosan beads [17], graphene oxide/chitosan composite fibers [18], magnetic Fe_3O_4/chitosan nanoparticles [19], zinc oxide impregnated chitosan beads [20], chitosan/clay/Fe_3O_4 [21], magnetic chitosan composites [22], magnetic chitosan/active charcoal composite [23], nano-ZnO/CT-CB [24], nano-TiO_2/CS/PNIPAAm [25], Zr-CCS/BT composite [26] and chitosan/grapheme oxide nano composite [27] have been used as an adsorbent material for the removal of heavy metals and dyes from wastewater.

In this study, the G, CSB and GCSB were chosen as the adsorbents. The adsorption behavior of MO onto G, CSB and GCSB were investigated. Batch sorption experiments were performed to evaluate the influence of pH, contact time, initial dye concentration and temperature. The Langmuir, Freundlich and Dubinin-Radushkevich isotherm models were applied to the experimental data. Kinetic studies were performed using pseudo-first-order and pseudo-second-order models. Thermodynamic parameters, such as Gibb's free energy (ΔG^o), enthalpy (ΔH^o), and entropy (ΔS^o), were also evaluated by Van't Hoff equation. Additionally, the adsorbents were characterized by FTIR, SEM and BET analyses.

2. Materials and methods

2.1. Materials

Chitosan (reagent grade, >85% deacetylation, low molecular weight of 50,000–190,000 g/mol) was purchased form the Sigma Chemical Co., USA. Methyl orange (MO) [formula weight: $C_{14}H_{14}N_3NaO_3S$, molecular weight: 327.3, λ_{max}: 464 nm] was purchased from Junsei Chemicals, Japan. The structure of the MO is shown in Fig. 1. Double deionized water (Milli-Q Millipore 18.2 MΩ cm^{-1} conductivity) was used throughout the work. A stock solution (1000 mg/L) was prepared by dissolving required amount of MO in double distilled water which was later diluted to desired concentrations. Ferric chloride, glacial acetic acid, potassium hydroxide, sodium hydroxide, hydrochloric acid and other reagents were of analytical grade. pH of MO solutions was adjusted by adding 0.1 M NaOH (or) 0.1 M HCl solution. MO concentrations were measured using a UV–Vis spectrophotometer (Optizen Pop, Korea) after appropriate dilution.

2.2. Preparation of the adsorbents

Goethite was prepared using a method based on the report of Schwertmann and Cornell [28]. The method was briefly described here under an 80 mL of the 0.2 M $FeCl_3$. $6H_2O$ is added to a 500 mL borosilicate glass bottle followed by the rapid addition of 20 mL of 2.5 M KOH solution. The resulting suspension was aged for 60 h at 70 °C where a yellow brown precipitate of goethite was formed. The supernatant solution was separated and goethite suspension was washed repeatedly with double distilled water and dried at 60 °C for 24 h in an oven then fine ground. The obtained product was named as goethite.

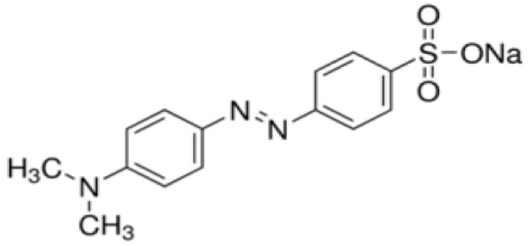

Fig. 1. Molecular structure of MO.

3.0 g chitosan powder was dissolved in a 100 mL of 2% (v/v) acetic acid aqueous solution. The homogeneous gel was obtained by stirring 4 h at room temperature. The chitosan gel was transferred drop wise into the 10% NaOH with continuous stirring. The obtained beads were immersed in fresh 10% NaOH and stirred mechanically for 4 h. Finally the beads were washed with double distilled water and dried in an oven at 60 °C for 24 h.

The chitosan solution (3% w/v) was prepared by dissolving chitosan powder (3 g) in an aqueous acetic acid solution (2% v/v). Then, goethite powder (0.34 g) was added into the chitosan solution and stirred vigorously for 6 h. Then followed the same procedure discussed in above paragraph to get GCSB. All adsorbents are stored in vacuumed desiccators for further MO adsorption studies.

2.3. Characterization of adsorbents

Fourier transform infrared spectroscopy (FT-IR) was recorded using a Fourier transform infrared spectrophotometer (Nicolet IS10, Thermo Scientific, USA). The scanning range of the scanning wavenumbers was 400–4000 cm^{-1}. For IR spectral studies, 10 mg of sample was mixed and ground with 100 mg of KBr and made into a pellet. The background absorbance was measured by using a pure KBr pellet. The morphological images of G, CSB and GCSB were taken using scanning electron microscope (JEOL, JSM-7600F, Japan). The acceleration voltage was 30.0 kV. The samples were first sputter-coated with homogeneous gold layer and then loaded onto a copper substrate. The BET surface area, pore volume and pore structure of G, CSB and GCSB were obtained from nitrogen adsorption data at 77 K using a gas adsorption analyzer (BELSORP, BEL Japan). Each sample was degassed at 323 K for 12 h to obtain a residual pressure < 10^{-6} mmHg. The specific surface areas and micro pore volume of the samples were calculated by the BET equation and D-R equation, respectively. The amounts of N_2 adsorbed at relative pressure ($P/P_o = 0.98$) were used to investigate the total pore volumes, which corresponded to the sum of the micropore and mesopore volumes.

2.4. Batch adsorption studies

In order to evaluate adsorption properties of G, CSB and GCSB for MO, a series of adsorption experiments including pH, kinetics, isotherms, temperature and thermodynamics were conducted. The effect of pH was studied in the range of 3.0 to 10.0. Sorption kinetic experiments were conducted with an initial concentration of 100 mg/L at room temperature. Samples were collected at various time intervals until the concentration of MO in the dilute phase become constant. The adsorption isotherm was obtained by varying the initial MO concentration between 10 and 100 mg/L. The effect of temperature on the adsorption of MO was investigated by controlling the temperature at 298, 308, 318, 328 and 338 K. At the end of adsorption, 1 mL sample was collected and centrifuged at 3000 rpm for 10 min. The filtrate was then collected in polythene tubes and diluted before measurement. The MO residual concentration was determined using UV–Vis spectrophotometer. Each experiment was duplicated under identical conditions, and the mean value was used. The amount of adsorbed MO was calculated by the difference between initial and final MO concentrations in the solutions, which can be expressed by the following equation:

$$q = \frac{C_i V_i - C_f V_f}{M} \quad (1)$$

where q is the amount of adsorbed MO (mg/g), C_i and C_f are the initial and final MO concentrations in the solution (mg/L), respectively, V_i and V_f are the initial and final (initial plus the volume of HCl or NaOH solutions added) solution volumes, respectively, and M is the mass of the adsorbent (g).

2.5. Desorption and regeneration studies

Desorption of MO from G, CSB and GCSB was investigated using different concentrations of NaOH (0.1–1.0 M). Fresh adsorbents were loaded with MO by agitating mixture of 0.1 g and 30 mL of 100 mg/L MO solution at pH 3.0 for 4 h. The MO loaded adsorbents were separated by centrifugation and the residual MO concentration was determined by UV–Vis spectrophotometer. The MO loaded adsorbents were washed gently with water to remove any unadsorbed dye and then dried. The desorption process was carried out by mixing 30 mL of each desorbing eluent with the dried loaded adsorbents and shaken for a predetermined time and the desorbed MO was determined by UV–Vis spectrophotometer. Adsorbents were washed repeatedly with deionized water to remove any residual desorbing solution. The sorbents were placed into MO solution for the succeeding adsorption cycle after drying to a constant weight. The cycles were repeated five times using the same adsorbents. The efficiency of desorbed dye from the adsorbent was calculated by using the following equation.

$$\text{Desorption efficiency} = \frac{\text{Amount of MO desorbed}}{\text{Amount of MO adsorbed}} \times 100 \quad (2)$$

3. Results and discussion

3.1. Characterization

The FTIR spectra of G (A), CSB (B), and GCSB (C) altogether are shown in Fig.2. In the spectra (A), a broad band appears around 3167 cm^{-1} is due to the presence of the OH stretching mode in α-FeOOH. The band at 1651 $cm^{-1}$is attributed to asymmetric stretching vibration of C═O groups. The bands at 1447 and 1337 cm^{-1} are assigned to the deformation vibration of —$CH_2$and —CH_3. A band at 1057 cm^{-1} is due to the C—O—C stretching vibrations. Two typical bands at 889 and 795 cm^{-1} can be ascribed to Fe—O—H bending vibrations. In the spectra (B), showed broad peak at 3481 cm^{-1} corresponds to N—H and hydrogen bonded O—H stretching vibration. The peak at 2867 cm^{-1} was assigned to the symmetric stretching of —CH_2 groups. The bands appearing at 1652 and 1380 cm^{-1} were assigned to C═O stretching vibration of amide group and C—O stretching of primary alcoholic group. The absorption band at 1068 cm^{-1} was attributed to the C—O vibrations (for bridge C—O—C stretching).In spectra (C),showed broad intense characteristic bands at 3457 and 1673 cm^{-1} corresponding to —OH stretching and bending vibrations of absorbed water as well as asymmetrical stretching vibrations of C═O group. However, weak symmetrical stretching and bending vibrations of —CH and C—O—C groups are also appeared near 1498, 1068 cm^{-1}. The absorption band at the low frequency zone of 500–700 cm^{-1} is assigned to the stretching vibration of Fe—O in goethite. The interaction between the amine groups of chitosan and the surface hydroxyl groups of goethite may be the expected reason for attachment of chitosan with goethite. The FTIR studies confirmed the presence of hydroxyl (—OH), amine (—NH_2) and carboxyl (—C═O) groups which may be the primary responsible sites for MO adsorption.

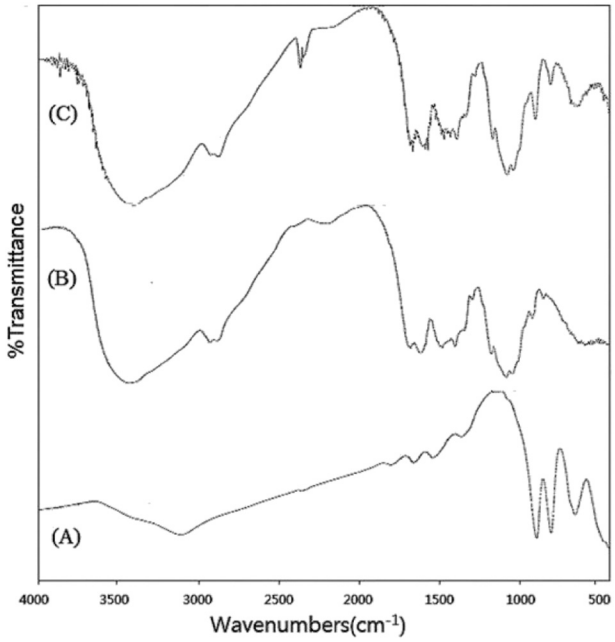

Fig. 2. FTIR spectra of: (A) G, (B) CSB and (C) GCSB.

The SEM images of G, CSB, and GCSB were shown in Fig. 3. The SEM image of G shows the presence of many irregular particles (Fig. 3A), which leads to give a rough surface for G. The SEM images of CSB and GCSB were nearly spherical in shape (Fig. 3B and C). The CSB has relatively smooth surfaces, whereas the GCSB was rough because of G. Rough surfaces are favorable for molecular diffusion and could provide a larger surface area for the adsorption of contaminants.

The Brunauer-Emmett-Teller (BET) surface area, pore volume and pore diameter of G, CSB, and GCSB were determined by BJH analysis. BET surface area, pore volume and pore diameter of G, CSB, and GCSB were presented in Table 1. The results revealed that the GCSB has the highest surface area, pore volume and pore diameter which was advantageous for MO adsorption. On the other hand, G and CSB had the smallest surface area, pore volume and pore diameter. Generally, an adsorbent with large surface area, high pore volume and high pore diameter has more exposed surface sites for dye adsorption [29]. Therefore, GCSB is more compatible for the enhanced removal of MO compared to G and CSB.

Fig. 4 shows the most possible schematic illustration of goethite impregnated with chitosan beads structure. Goethite act as cross-linking agents to link the chitosan chains through the formation of both strong primary covalent bonds as well as hydrogen bondings.

3.2. Effect of pH

The pH of the solution greatly influences the adsorption process; it determines the surface charge of the adsorbent and the state of adsorbate in solution. The effect of pH on MO adsorption by G, CSB and GCSB at different pH values was studied and the results were shown in Fig. 5. It was observed that the adsorption capacities of G, CSB and GCSB decreased from 51.4 to 8.7 mg/g, from 67.9 to16.3 mg/g and from 81 to 24.7 mg/g, respectively, with an increase in the pH of the MO solution from 3 to 10. The maximum adsorption capacity of MO was achieved at pH 3.0 for all the adsorbents (G, CSB and GCSB). Under acidic conditions (below pH 3.0) the chitosan undergoes dissolution [30]. Due to this dissolution, experiments were conducted above pH 3.0. At low pH values, the surface of the adsorbents was positively charged and partial —NH_2 groups in the adsorbents were protonated to —NH_3^+ groups. Thus, the electrostatic attraction between the negatively charged MO anions and the positively charged surface of the adsorbents was enhanced, resulting in high sorption capacity.

Adsorption mechanism may be as follows:

$$R-NH_2 + H^+ \leftrightarrow R-NH_3^+$$

$$MO-SO_3Na \rightarrow MO-SO_3^- + Na^+$$

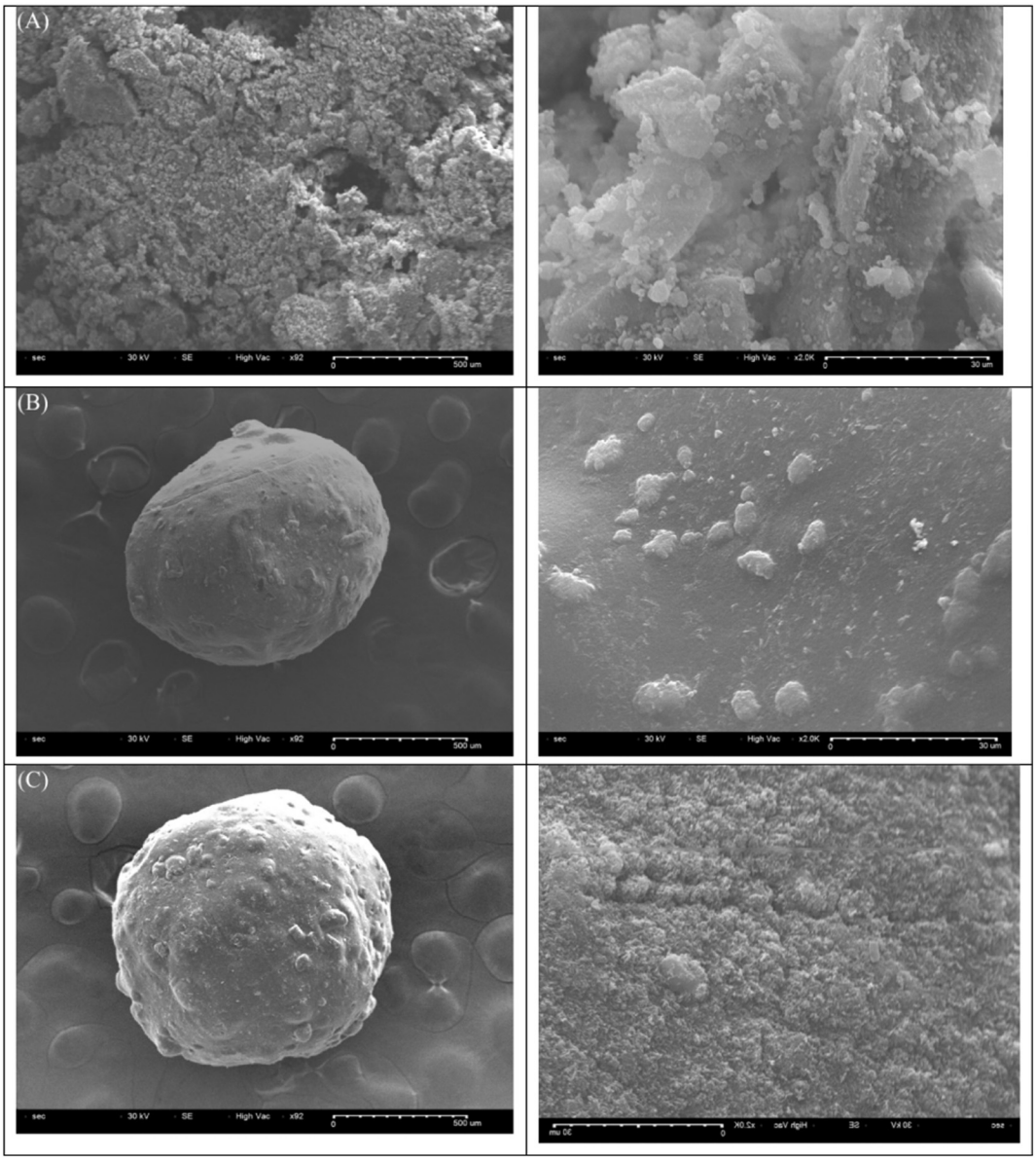

Fig. 3. SEM images of: (A) G, (B) CSB and (C) GCSB.

$$R-NH_3^+ + MO-SO_3^- \rightarrow R-NH_3^+O_3S-MO$$

However, with increasing pH values, the number of the negatively charged sites increased, and the number of the positively charged sites decreased. When the pH value was higher than 4.0, the surface of the adsorbents were negatively charged. The electrostatic repulsive force became dominant, thereby weakening the adsorption of MO on the adsorbents and consequently reducing the sorption of MO. In addition, lower adsorption of MO at alkaline pH was attributed to the competition of hydroxyl ions in the solution with the dye anions for adsorptive sites [31].

Table 1
Surface parameters of G, CSB and GCSB.

Adsorbent	Surface area (m^2/g)	Pore volume (cm^3/g)	Pore diameter (nm)
G	4.37	0.0159	10.24
CSB	10.81	0.1165	16.69
GCSB	17.81	0.2145	26.18

3.3. Effect of contact time

Equilibrium time plays a vital role and is one of the most important parameters in kinetic modelling of dyes during the design of a low cost wastewater treatment system. Fig. 6 illustrates the adsorption capacity of G, CSB and GCSB in MO solutions as a function of contact time from 0 to 480 min at room temperature. It has been observed that the rate of adsorption capacity of MO was rapid in the beginning, proceeded at a slower rate and finally attained equilibrium at about 180 min. This is due to the availability of the larger surface area of the adsorbent in the beginning. As the surface adsorption sites become exhausted, the uptake rate is controlled by the rate at which the adsorbate is transported from the exterior to interior sites of the adsorbent [32]. The adsorption occurred due to attractive electrostatic attractions, Van der Waals forces and fast diffusion onto the external surface of the adsorbent.

3.4. Adsorption kinetic models

Kinetics is one of the key aspects used in the evaluation of adsorption as a unit process. The residence time for dye adsorption can be

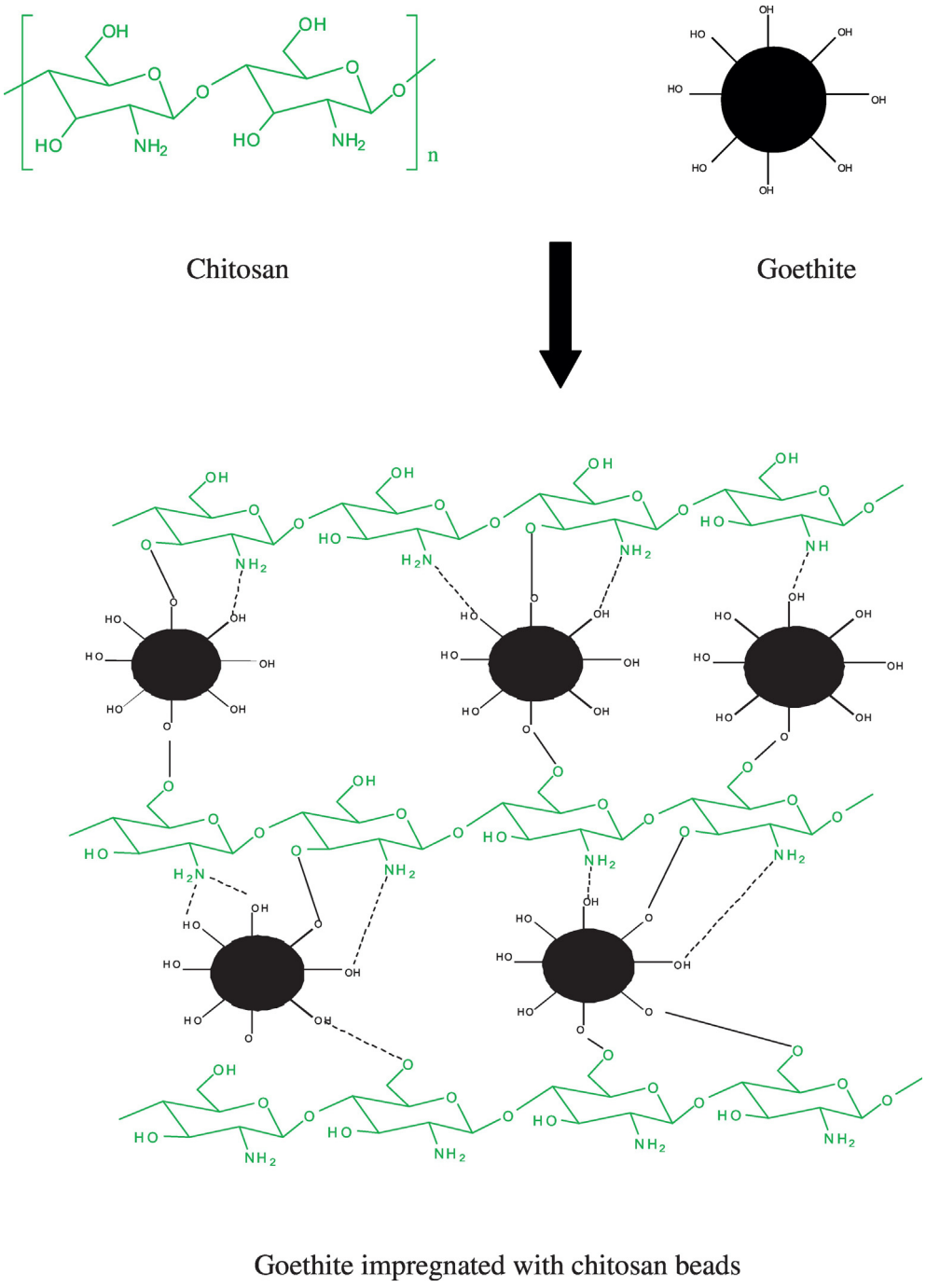

Fig. 4. The proposed structure of goethite impregnated chitosan beads made from chitosan and goethite.

determined by kinetics examination of the equilibrium data. In this study, the kinetics of the MO adsorption onto G, CSB and GCSB from the solution was investigated by two well-known kinetic models, namely, pseudo-first-order and pseudo-second-order. The non-linear forms of these two models are expressed by the following equations:

Pseudo-first-order [33]

$$q_t = q_1(1- \exp(-k_1 t)) \quad (3)$$

Pseudo-second-order [34]

$$q_t = \frac{q_2^2 k_2 t}{1 + q_2 k_2 t} \quad (4)$$

where, q_1 and q_2 are the amount of dye adsorbed at equilibrium (mg/g), q_t is the amount of dye adsorbed at time t (mg/g), k_1 is the pseudo-first-order equilibrium rate constant (1/min) and k_2 is the pseudo-second-order equilibrium rate constant (g/mg min). Values of pseudo-first-order and pseudo-second-order rate constants and correlation coefficient are given in the Table 2 and non-linear plots are shown in Fig. 7. The results indicated that among these two models, the pseudo-second-order kinetic model had higher R^2 values and experimental q_e values that agree well with the calculated q_2 values. The low R^2 values for pseudo-first-order model indicated that this model did not fit the data well. Furthermore, for the pseudo-first-order kinetic model, the experimental q_e was not in good agreement with the calculated q_1 values. Therefore, the pseudo-second-order

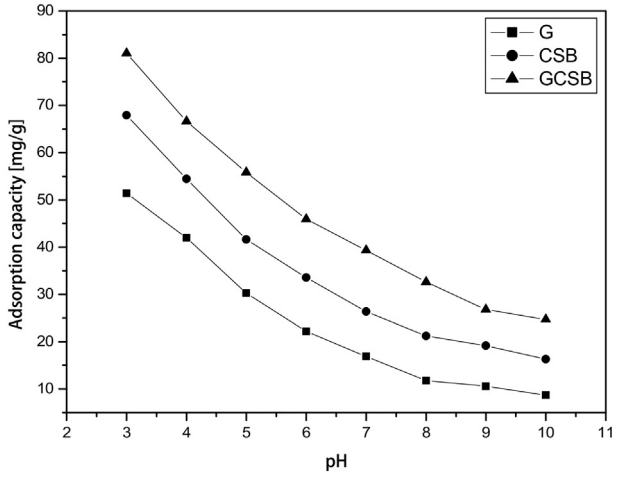

Fig. 5. Effect of pH on the adsorption of MO by G, CSB and GCSB.

kinetic model provided the best description of the MO adsorption mechanism.

3.5. Adsorption isotherm models

Successful application of the adsorption technique demands the studies based on various adsorption isotherm models, because adsorption isotherm models clearly depict the relationship between the concentration of dye in solution and the amount of dye adsorbed on the solid phase when both phases are in equilibrium [35]. In this study, the three adsorption isotherm models, Langmuir, Freundlich and Dubinin-Radushkevich (D-R) isotherm equations were used to describe the experimental sorption data.

3.5.1. Langmuir isotherm

The Langmuir isotherm [36] assumes monolayer adsorption onto a surface containing a finite number of adsorption sites of uniform strategies of adsorption with no transmigration of adsorbate in the plane of surface. The non-linear form of Langmuir adsorption isotherm is given below.

$$q_e = \frac{q_m K_L C_e}{1 + K_L C_e} \tag{5}$$

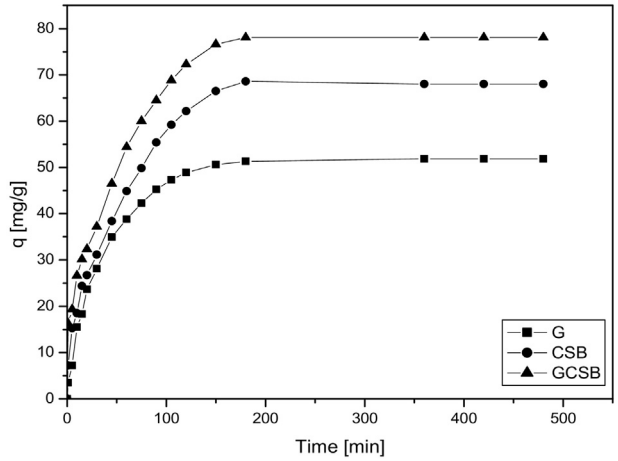

Fig. 6. Effect of contact time on the adsorption of MO onto G, CSB and GCSB.

Table 2
Kinetic parameters of pseudo-first-order and pseudo-second-order models for MO adsorption on G, CSB and GCSB.

Adsorbent	q_e, exp. (mg/g)	Pseudo-first-order			Pseudo-second-order		
		q_1, cal (mg/g)	k_1 (1/min)	R^2	q_2, cal (mg/g)	k_2 (g/mg min)	R^2
G	51.3	57.8	0.0270	0.9853	51.0	0.0004	0.9953
CSB	67.0	77.6	0.0211	0.9739	67.6	0.0003	0.9939
GCSB	78.1	87.4	0.0203	0.9483	76.4	0.0003	0.9965

where q_e is the amount of adsorption at equilibrium (mg/g), q_m is the maximum adsorption capacity of adsorbate per unit mass of adsorbent (mg/g), C_e is the equilibrium concentration of the adsorbate (mg/L) and K_L is the Langmuir constant related to the

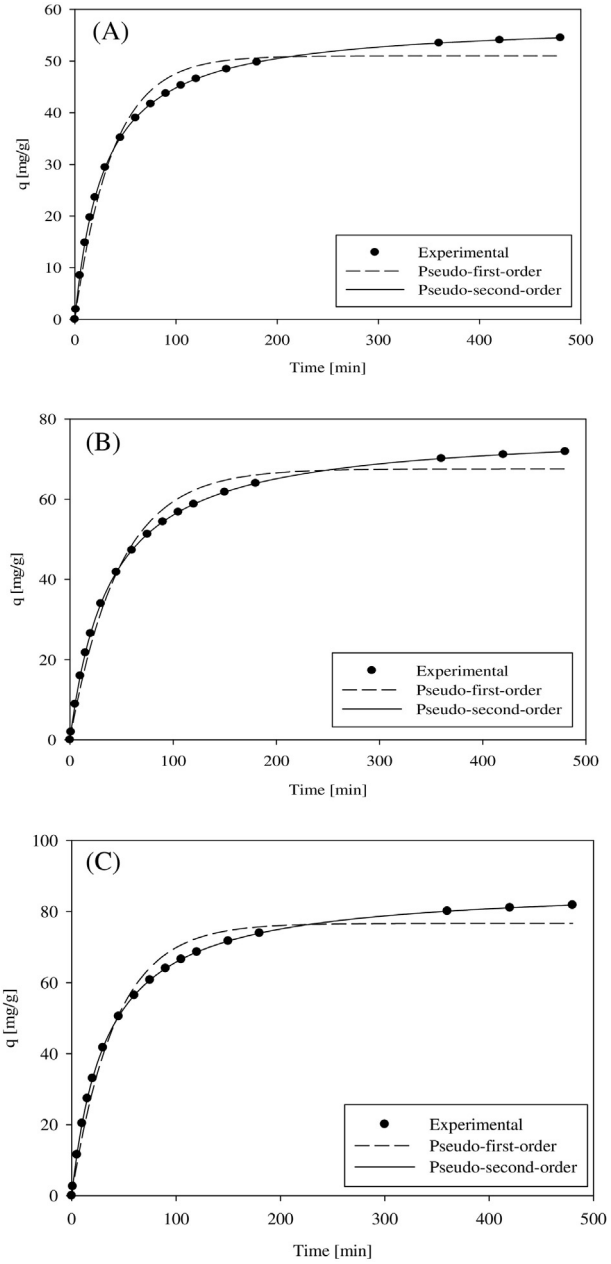

Fig. 7. Adsorption kinetics of MO onto (A) G, (B) CSB and (C) GCSB.

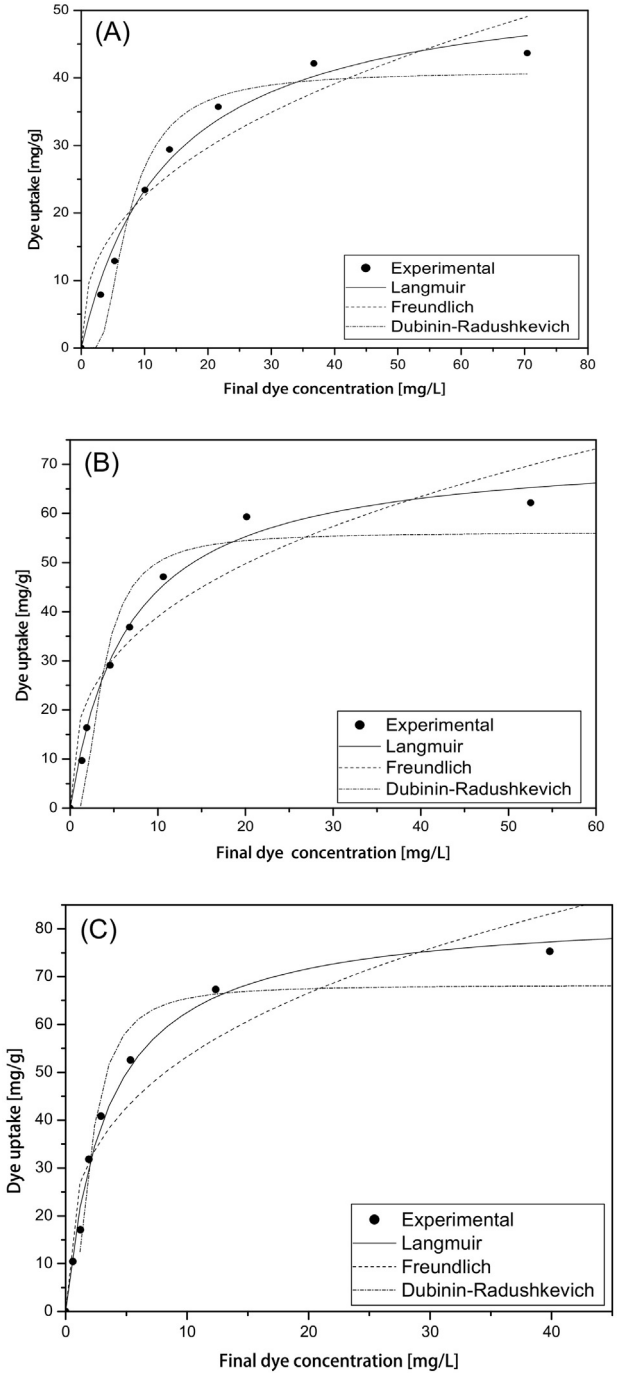

Fig. 8. Adsorption isotherms of MO onto the (A) G, (B) CSB and (C) GCSB.

adsorption equilibrium (L/mg). The maximum adsorption capacity of MO was found to be 55, 73 and 84 mg/g for G, CSB and GCSB, respectively.

The essential characteristics of the Langmuir isotherm may be expressed in terms of a dimensionless constant called separation factor (R_L) and is given by the following equation:

$$R_L = \frac{1}{1 + K_L C_0} \tag{6}$$

where R_L is the equilibrium constant that indicates the type of adsorption, K_L is the Langmuir constant (L/mg) and C_o is the initial dye concentrations (mg/L). R_L values lies between 0 and 1 for favorable adsorption, $R_L = 1$ represents linear adsorption, $R_L = 0$ indicates the irreversible adsorption process and $R_L > 1$ represents unfavorable adsorption. The values of R_L are all in the range of 0–1, which indicate the favorable adsorption of MO onto G, CSB and GCSB. This means that the equilibrium isotherms can be well described by the Langmuir isotherm model, and the adsorption process is monolayer adsorption onto a surface with finite number of identical sites, which are homogeneously distributed over the adsorbents surface.

3.5.2. Freundlich isotherm

Freundlich isotherm [37] can be applied to an adsorption system when the number of adsorption sites exceeds the number of contaminant molecules/ions. The isotherm thus describes multilayer and physical adsorption over the heterogeneous surface. According to Freundlich isotherm, each adsorbing site has specific bond energy and stronger binding site is occupied first, and adsorption energy decrease exponentially upon the completion of the process. The non-linear form of Freundlich isotherm is given by the following equation:

$$q_e = K_f C_e^{1/n} \tag{7}$$

where K_f (mg/g) and n are the Freundlich constants which represent adsorption capacity at unit concentration and adsorption intensity, respectively. Both K_f and n predict the feasibility of adsorption process. Freundlich constants, n, is exponent which is measure of adsorption intensity or surface heterogeneity, whose value lies in the range 1–10 for favorable adsorption phenomenon. K_f values for MO come out to be 8.98, 17.4 and 25.4 mg/g for G, CSB and GCSB, respectively. The n values were 2.51, 2.85 and 3.11 for G, CSB and GCSB, respectively, thus n values in the range 1–10, provided information about favorability of MO adsorption onto G, CSB and GCSB.

3.5.3. Dubinin-Radushkevich isotherm

Dubinin-Radushkevich (D-R) isotherm [38], is more general than Langmuir isotherm, since it does not assumes a homogeneous surface or constant adsorption potential. This isotherm has been extensively used to distinguish the physical and chemical adsorption. The non-linear form of D-R isotherm is represented as follow:

$$q_e = Q_m \exp\left(-K\left[RT \ln\left(1 + \frac{1}{C_e}\right)\right]^2\right) \tag{8}$$

$$q_e = Q_m = \exp(-K\varepsilon^2) \tag{9}$$

where Q_m is the maximum amount of the dye ion that can be sorbed onto a unit weight of sorbent, ε is the Polanyi potential which is equal

Table 3
Parameters of isotherm models for adsorption of MO on G, CSB and GCSB.

Adsorbent	Langmuir				Freundlich				Dubinin-Radushkevich				
	q_m (mg/g)	K_L (L/mg)	R^2	χ^2	K_f (mg/g)	n	R^2	χ^2	Q_m (mg/g)	K	E (kJ/mol)	R^2	χ^2
G	55	0.073	0.9951	4.6	8.98	2.51	0.9201	19.3	40.9	0.048	3.2	0.9167	24.5
CSB	73	0.152	0.9899	6.2	17.4	2.85	0.9103	55	56.1	0.025	4.5	0.8631	67.5
GCSB	84	0.294	0.9908	7.9	25.4	3.11	0.9349	46.6	68.2	0.015	5.8	0.9024	83.6

to $RT \ln(1 + 1/Ce)$, R is the gas constant 8.314 kJ/mol K, T is the temperature (K) and C_e is the dye equilibrium concentration. The mean free energy of sorption E (kJ/mol) required to transfer one mole of dye from the infinity in the solution to the surface of G, CSB and GCSB can be determined by the following equation:

$$E = \frac{1}{\sqrt{2K}} \tag{10}$$

The value of E is very useful in predicting the type of adsorption and if the value is <8 kJ/mol, then the adsorption is physical in nature and if it is in between 8 and 16 kJ/mol, then the adsorption is due to exchange of ions [39]. In the present study, the values of E < 8.0 kJ/mol, indicated adsorption of MO onto G, CSB and GCSB as physical process.

The non-linear form of adsorption data fitted to the Langmuir, Freundlich and Dubinin-Radushkevich isotherm models are presented in Fig. 8. From this non-linear fitting, some parameters of each model can be determined and the results are presented in Table 3. Compared to Freundlich and Dubinin-Radushkevich model, the Langmuir isotherms model employed to describe the adsorption process fits well due to the higher value of R^2, indicating the monolayer coverage of MO onto G, CSB and GCSB. The maximum adsorption of G, CSB and GCSB for MO obeys from Langmuir isotherm model.

The Chi-square analysis was used for comparing all isotherms on the abscissa ad ordinate. The equation for evaluating the best fit model is to be evolved as:

$$\chi^2 = \sum \left(\frac{(q_e - q_{e,m})^2}{q_{e,m}} \right) \tag{11}$$

where $q_{e,m}$ equilibrium capacity obtained by calculating from model (mg/g) and q_e was the equilibrium capacity (mg/g) from the experimental data. If data from model were similar to the experimental data, χ^2 would be a small number and vice versa. The values of χ^2 of each model were shown in Table 3. In this study, the low Chi-square values suggest that the Langmuir isotherm model is better fitted, followed by Freundlich and Dubinin-Radushkevich isotherm models.

3.6. Comparison with other adsorbents

For further comparison with other various adsorbents, the adsorption capacity (q_{max}; mg/g) of different adsorbents reported in the literature [40–55]are listed in Table 4. According to this table, the adsorption capacities of the G, CSB and GCSB were much higher than that of the reported adsorbents, indicating that the G, CSB and GCSB have important potential for the adsorption MO from aqueous solution.

Table 4
Comparison of MO adsorption capacity of G, CSB and GCSB with that of various adsorbents.

Adsorbent	q_{max} (mg/g)	Reference
Functionalized-CNTs loaded TiO_2	42.85	[40]
Calcium alginate MWNTs	12.5	[41]
Chitosan/alumina composite	33	[42]
γ- Fe_2O_3/chitosan composite films	29.41	[43]
γ- Fe_2O_3/MWCNTs/chitosan	60.5–66.1	[44]
γ- Fe_2O_3/SiO_2/CS composite	34.29	[45]
γ- Fe_2O_3 crosslinked chitosan composite	29.46	[46]
Chitosan/organic rectorite	5.56	[47]
Zirconium-immobilized bentonite	44.13	[48]
Al/CTAB-bent	42.37–47.55	[49]
Zeolite NaA/CuO	79.49	[50]
KGM/GO	51.6	[51]
FA modified $Ca(OH)_2$/Na_2FeO_4	14.76	[52]
Magnetic MWCNTs	10.89	[53]
CS/Mt.-OREC microspheres	5.56	[54]
Protonated cross-linked chitosan	89.30	[55]
G	55	This study
CSB	73	This study
GCSB	84	This study

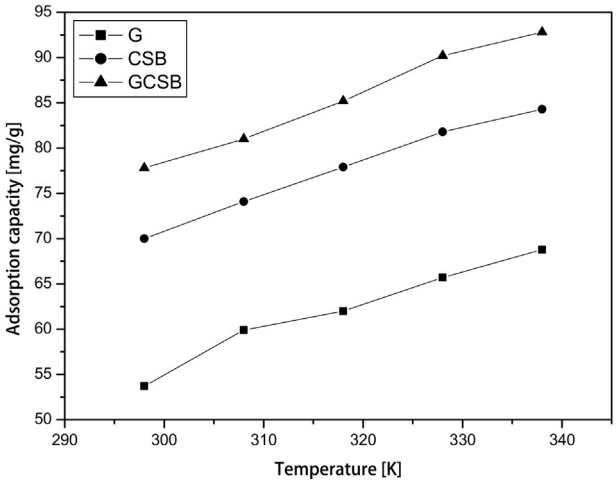

Fig. 9. Effect of temperature on MO of the G, CSB and GCSB.

3.7. Effect of temperature

Temperature is an extremely important parameter controlling the adsorption process. The temperature is an indicator for the adsorption nature whether it is an endothermic or exothermic process. Fig. 9 shows MO adsorption onto G, CSB and GCSB at different temperatures. The MO adsorption capacity presents a significant increasing trend with the rise in temperature (298–338 K), and it reached up to 68.8, 84.3 and 92.8 mg/g for G, CSB and GCSB, respectively at 338 K. The results suggest that MO adsorption on the adsorbents was favored at higher temperatures within the appropriate temperature range and the G, CSB and GCSB can be used as high efficiency adsorbents for the removal MO from aqueous solution. The reason may be ascribed to the mobility of MO molecules increases with the rise in temperature and more dye molecules can interact with the active sites on G, CSB and GCSB. The MO adsorption capacities increased with increase of temperature, indicating the endothermic nature of adsorption.

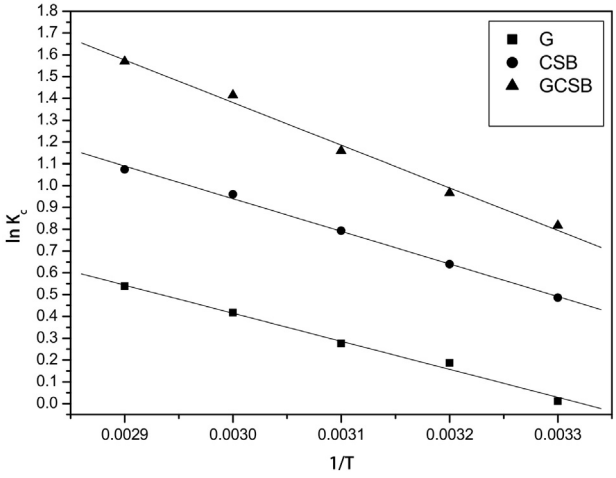

Fig. 10. Plot of ln K_c vs 1/T for the estimation of thermodynamic parameters for adsorption of MO onto G, CSB and GCSB.

Table 5
Thermodynamic parameters of MO on G, CSB and GCSB at various temperatures.

Adsorbent	Temp. (K)	ΔG° (kJ/mol)	ΔS° (kJ/mol K)	ΔH° (kJ/mol)
G	298	−0.0273		
	308	−0.4788		
	318	−0.7297	0.036	10.7
	328	−0.1372		
	338	−1.5147		
CSB	298	−1.2041		
	308	−1.6363		
	318	−2.0966	0.046	12.4
	328	−2.6179		
	338	−3.0181		
GCSB	298	−2.0242		
	308	−2.4736		
	318	−3.0642	0.061	16.3
	328	−3.8587		
	338	−4.4119		

The temperature affects through the entropy (ΔS^o) and the enthalpy (ΔH^o), in accordance with the van't Hoff Eq. (13) and the Gibb's free energy ΔG^o in Eq. (14):

$$K_c = \frac{C_{Ae}}{C_e} \tag{12}$$

$$\ln K_c = \frac{\Delta S^o}{R} - \frac{\Delta H^o}{RT} \tag{13}$$

$$\Delta G^o = -RT\ \ln K_c \tag{14}$$

where K_c is the ratio of C_{Ae}, the solid phase concentration of MO at equilibrium (mg/L), to C_e, the equilibrium concentration of MO in solution (mg/L), R is the universal gas constant (8.314×10^{-3} kJ/mol K), and T is the absolute temperature (K). The values of entropy (ΔS^o) and the enthalpy (ΔH^o) were obtained from the slope and intercept of the van't Hoff plots shown in Fig. 10, and the Gibb's free energy (ΔG^o) was calculated from Eq. (14). The obtained values of the thermodynamic parameters of MO adsorption onto G, CSB and GCSB are summarized at various temperatures in Table 5. The negative values of Gibbs free energy change (ΔG^o) show that the adsorption of MO onto G, CSB and GCSB are extremely favorable. Moreover, ΔG^o values were found to decrease with the rise of temperature confirmed the spontaneous nature of the adsorption process at elevated temperatures, this may be explained that the enlargement of adsorbent pores and more surface activation. Generally, a value of ΔG^o in between 0 and −20 kJ/mol is consistent with electrostatic interaction between adsorption sites and the adsorbing ion (physical adsorption) while a more negative ΔG^o value ranging from −80 to −400 kJ/mol indicates that the adsorption involves charge sharing or transferring from the adsorbent surface to the adsorbing ion to form a coordinate bond (chemisorption) [56]. As shown in Table 5, the magnitude of ΔG^o indicates a typical physical process. The positive values of ΔH^o indicate that the adsorption process was endothermic and higher temperature was more favorable to the adsorption. The positive ΔS^o values suggest the increased randomness at the solid-solution interface during the fixation of dye on adsorbent surface.

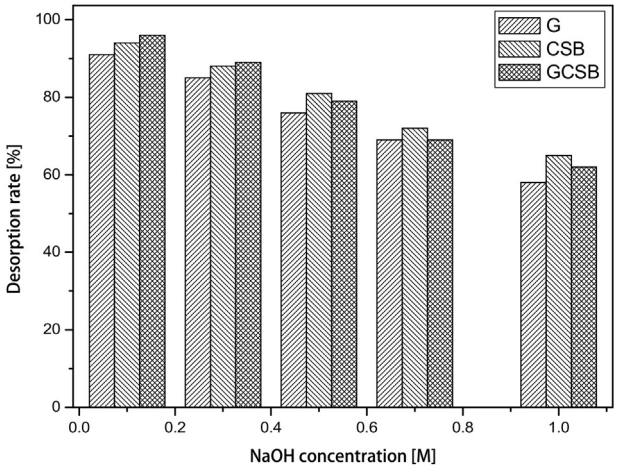

Fig. 11. Effect of NaOH concentration on desorption of MO from the G, CSB and GCSB.

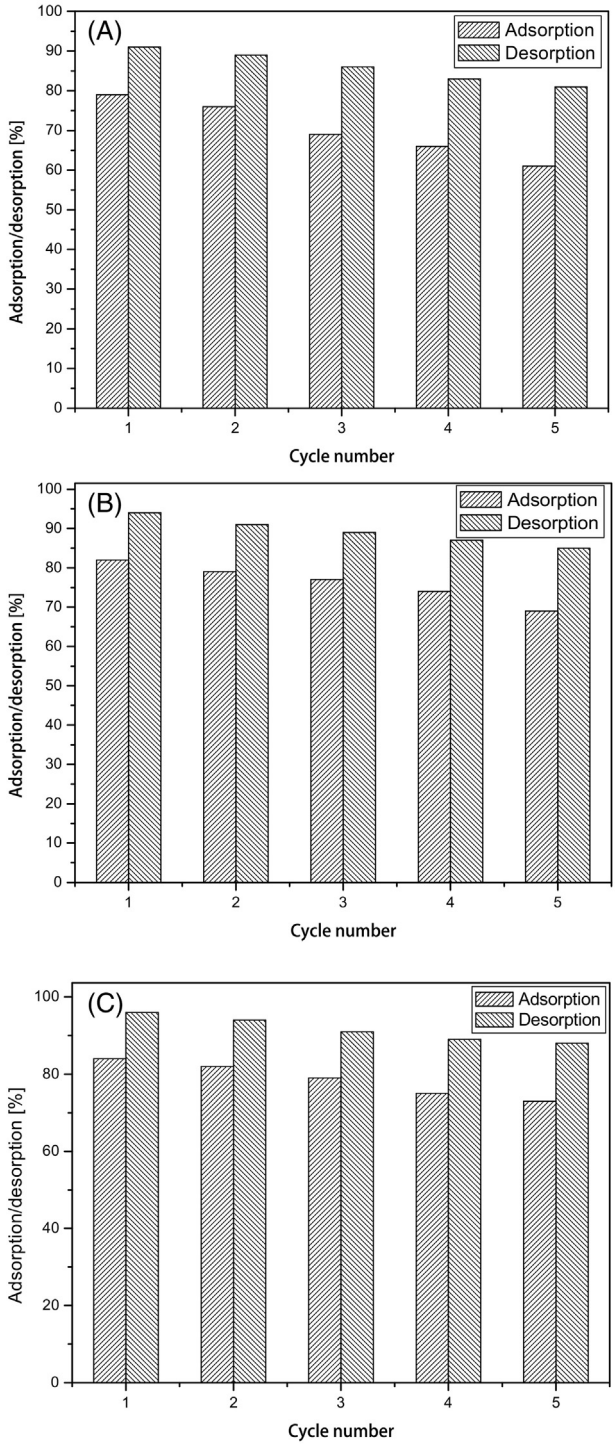

Fig. 12. Methyl orange adsorption–desorption cycles: (A) G, (B) CSB and (C) GCSB.

3.8. Desorption and regeneration studies

The recycling and regeneration of adsorbent is important for the practical application of adsorption process. The adsorbents having regeneration ability are considered as cost effective and applicable at pilot scale. To test the suitability and stability of the adsorbent, it was subjected to successive adsorption and desorption cycles. Dilute solutions of bases could be employed for desorption studies. Here, NaOH solution was selected as an eluent to desorb MO from the MO-loaded G, CSB and GCSB. Various concentrations of NaOH (0.1–1.0 M) were used as desorbing media for the regeneration of G, CSB and GCSB and results are presented in Fig. 11. The results showed that with increase in concentration of NaOH solution the desorption efficiency decreased. From Fig. 10, the desorption efficiency of 91% for G, 94% for CSB and 96% for GCSB were observed, when the recovery of MO was obtained by 0.1 M NaOH. Hence, 0.1 M NaOH was chosen as a suitable concentration for the regeneration of MO. The regenerated adsorbents were reused for adsorption-desorption cycles and the data were shown in Fig. 12. In each cycle, the adsorbents were filtered and repeatedly washed with deionized water after each desorption to eliminate the excess of base. The results showed that the desorption percentage of MO decreased to about 81, 85 and 88% after five cycles for G, CSB and GCSB, respectively. It can be concluded that G, CSB, and GCSB can be used repeatedly with negligible loss in their adsorption capacity for the representative MO.

4. Conclusions

In this study, G, CSB and GCSB are employed as novel adsorption material for the removal of MO from aqueous systems. The effects of the pH, contact time, initial MO concentration and temperature were also examined. FTIR spectra of the G, CSB and GCSB are clearly elucidated the nature of the functional groups (—OH, —NH_2 and —C═O) onto the surface are involved in the adsorption mechanism for the removal of MO. The experimental data of MO sorption onto G, CSB and GCSB were well fitted by Langmuir isotherm model. The maximum adsorption capacities were found to be 55, 73 and 84 mg/g at pH 3.0 for G, CSB and GCSB, respectively. The adsorption kinetics followed the pseudo-second-order model for all the systems. Further, the increase in temperature favored the removal of MO and the sorption process was found to be spontaneous and endothermic in nature. Regeneration studies showed that up to five cycles G, CSB and GCSB can be effectively utilized for the recovery of MO. These results show that G, CSB and GCSB are potential adsorbents for removing MO from aqueous solution.

References

[1] B. Zhao, X. Zhang, C. Dou, R. Han, Adsorption property of methyl orange chitosan coated on quartz sand in batch mode, Desalin. Water Treat. 55 (2015) 1598–1608.
[2] P. Mokhtari, M. Ghaedi, K. Dashtian, M.R. Rahimi, M.K. Purkait, Removal of methyl orange by copper sulfide nanoparticles loaded activated carbon: kinetic and isotherm investigation, J. Mol. Liq. 219 (2016) 299–305.
[3] S. Agarwal, I. Tyagi, V.K. Gupta, M. Ghaedi, M. Masoomzade, A.M. Ghaedi, B. Mirtamizdoust, Kinetics and thermodynamics of methyl orange adsorption from aqueous solutions-artificial neural network-particle swarm optimization modeling, J. Mol. Liq. 218 (2016) 354–362.
[4] G. Leon, F. Garcia, B. Miguel, J. Bayo, Equilibrium, kinetic and thermodynamic studies of methyl orange removal by adsorption onto granular activated carbon, Desalin. Water Treat. 57 (2016) 17104–17117.
[5] S. Hosseini, M.A. Khan, M.R. Malekbala, W. Cheah, T.S.Y. Choong, Carbon coated monolith, a mesoporous material for the removal of methyl orange from aqueous phase: adsorption and desorption studies, Chem. Eng. J. 171 (2011) 1124–1131.
[6] K. Li, P. Li, J. Cai, S. Xiao, H. Yang, A. Li, Efficient adsorption of both methyl orange and chromium from their aqueous mixtures using a quaternary ammonium salt modified chitosan magnetic composite adsorbent, Chemosphere 154 (2016) 310–318.
[7] M. Khadhraoui, H. Trabelsi, M. Ksibi, S. Bouguerra, B. Elleuch, Descoloration and detoxicification of a congo red dye solution my means of ozone treatment for a possible water reuse, J. Hazard. Mater. 161 (2009) 974–981.
[8] R. Rakhunde, L. Deshpande, H. Juneja, Chemical speciation of chromium in water: a review, Crit. Rev. Environ. Sci. Technol. 42 (2012) 776–810.
[9] M.D. Murcia, M. Gomez, E. Gomez, J.L. Gomez, N. Christofi, Photodegradation of congo red using XeBr, KrCl and Cl_2 barrier discharge excilamps: a kinetics study, Desalination 281 (2011) 364–371.
[10] M.F. Elahmadi, N. Bensalah, A. Gadri, Treatment of aqueous wastes contaminated with congo red dye by electrochemical oxidation and ozonation processes, J. Hazard. Mater. 168 (2009) 1163–1169.
[11] M. Chafi, B. Gourich, A.H. Essadki, C. Vial, A. Fabregat, Comparison of electrocoagulation using iron and aluminium electrodes with chemical coagulation for the removal of highly soluble acid dye, Desalination 281 (2011) 285–292.
[12] M. Herrero, D.C. Stuckey, Bioaugmentation and its application in wastewater treatment: a review, Chemosphere 140 (2015) 119–128.
[13] G. Ciardelli, L. Corsi, M. Marcucci, Membrane separation for wastewater reuse in the textile industry, Resour. Conserv. Recycl. 31 (2000) 189–197.
[14] V.N. Tirtom, A. Dincer, S. Becerik, T. Aydemir, A. Celik, Comparative adsorption of Ni(II) and Cd(II) ions on epichlorohydrin crosslinked chitosan-clay composite beads in aqueous solution, Chem. Eng. J. 197 (2012) 379–386.
[15] L.X. Zeng, Y.F. Chen, Q.Y. Zhang, Y. Kang, J.W. Luo, Adsorption of congo red by crosslinked chitosan resins, Desalin. Water Treat. 52 (2014) 7733–7742.
[16] B. Liu, D. Wang, H. Li, Y. Xu, L. Zhang, As(III) removal from aqueous solution using α-Fe_2O_3 impregnated chitosan beads with As(III) as imprinted ions, Desalination 272 (2011) 286–292.
[17] J. Wang, W. Xu, L. Chen, X. Huang, J. Liu, Preparation and evaluation of magnetic nanoparticles impregnated chitosan beads for arsenic removal from water, Chem. Eng. J. 251 (2014) 25–34.
[18] Y. Li, J. Sun, Q. Du, L. Zhang, X. Yang, S. Wu, Y. Xia, Z. Wang, L. Xia, A. Cao, Mechanical and dye adsorption properties of graphene oxide/chitosan composite fibers prepared by wet spinning, Carbohydr. Polym. 102 (2014) 755–761.
[19] C. Cao, L. Xiao, C. Chen, X. Shi, Q. Cao, L. Gao, In situ preparation of magnetic Fe_3O_4/chitosan nanoparticles via a novel reduction-precipitation method and their application in adsorption of reactive azo dye, Powder Technol. 260 (2014) 90–97.
[20] M.H. Farzana, S. Meenakshi, Visible light-driven photoactivity of zinc oxide impregnated chitosan beads for the detoxification of textile dyes, Appl. Catal. A Gen. 503 (2015) 124–134.
[21] D.W. Cho, B.H. Jeon, C.M. Chon, F.W. Schwartz, Y. Jeong, H. Song, Magnetic chitosan composite for adsorption of cationic and anionic dyes in aqueous solution, J. Ind. Eng. Chem. 28 (2015) 60–66.
[22] D.H.K. Reddy, S.M. Lee, Application of magnetic chitosan composites for the removal of toxic metal and dyes from aqueous solutions, Adv. Colloid Interf. Sci. 201-202 (2013) 68–93.
[23] K. Karaer, I. Kaya, Synthesis, characterization of magnetic chitosan/active charcoal composite and using at the adsorption of methylene blue and reactive blue 4, Microporous Mesoporous Mater. 232 (2016) 26–38.
[24] S. Cinar, U.H. Kaynar, T. Aydemir, S.C. Kaynar, M. Ayvacikli, An efficient removal of RB5 from aqueous solution by adsorption onto nano-ZnO/chitosan composite beads, Int. J. Biol. Macromol. 96 (2017) 459–465.
[25] J. Zhou, B. Hao, L. Wang, J. Ma, W. Cheng, Preparation and characterization of nano-TiO_2/chitosan/poly(*N*-isopropylacrylamide) composite hydrogel and its application for removal of ionic dyes, Sep. Purif. Technol. 176 (2017) 193–199.
[26] L. Zhang, P. Hu, J. Wang, Q. Liu, R. Huang, Adsorption of methyl orange (MO) by Zr(IV)-immobilized cross-linked chitosan/bentonite composite, Int. J. Biol. Macromol. 81 (2015) 818–827.
[27] M.A. Kamal, S. Bibi, S.W. Bokhari, A.H. Siddique, T. Yasin, Synthesis and adsorptive characteristics of novel chitosan/graphene oxide nanocomposite for dye uptake, React. Funct. Polym. 110 (2017) 21–29.
[28] U. Schwertmann, R.M. Cornell, Iron oxides in the laboratory, Preparation and Characterization, second ed.VCH Publication, Weinheim, 1996.
[29] H.R. Mahmoud, S.M. Ibrahim, S.A. El-Molla, Textile dye removal from aqueous solutions using cheap MgO nanomaterials: adsorption kinetics, isotherm studies and thermodynamics, Adv. Powder Technol. 27 (2016) 223–231.
[30] K. Swayampakula, V.M. Boddu, S.K. Nadavala, K. Abburi, Competitive adsorption of Cu(II), Co(II) and Ni(II) from their binary and tertiary aqueous solutions using chitosan-coated perlite beads as biosorbent, J. Hazard. Mater. 171 (2009) 680–689.
[31] H. Deng, Z. Wei, X.N. Wang, Enhanced adsorption of active brilliant red X-3B dye on chitosan molecularly imprinted polymer functionalized with Ti(IV) as Lewis acid, Carbohydr. Polym. 157 (2017) 1190–1197.
[32] V.K. Gupta, D. Pathania, S. Sharma, S. Agarwal, P. Singh, Remediation and recovery of methyl orange from aqueous solution onto acrylic acid grafted *Ficus carica* fiber: isotherms, kinetics and thermodynamics, J. Mol. Liq. 177 (2013) 325–334.
[33] S. Lagergren, Zur theorie der sogenannten adsorption geloster stoffe, K. Sven. Vetenskapsakad. Handl. 24 (1898) 1–39.
[34] Y.S. Ho, G. McKay, Pseudo-second order model for sorption processes, Process Biochem. 34 (1999) 451–465.
[35] J. Shu, Z. Wang, Y. Huang, N. Huang, C. Ren, W. Zhang, Adsorption removal of congo red from aqueous solution by polyhedral Cu_2O nanoparticles: kinetics, isotherms, thermodynamics and mechanism analysis, J. Alloys Compd. 633 (2015) 338–346.
[36] I. Langmuir, The adsorption of gases on plane surfaces of glass, mica and platinum, J. Am. Chem. Soc. 40 (1918) 1361–1403.
[37] H.M.F. Freundlich, Uber die adsorption in lasugen, J. Phys. Chem. 57 (1906) 385–470.
[38] M.M. Dubinin, L.V. Radushkevich, Equation of the characteristic curve of activated charcoal, Proc. Acad. Sci. USSR 55 (1947) 331–333.
[39] M. Ghasemi, M. Naushad, N. Ghasemi, Y. Khosravi-fard, Adsorption of Pb(II) from aqueous solution using new adsorbents prepared from agricultural waste: adsorption isotherm and kinetic studies, J. Ind. Eng. Chem. 20 (2014) 2193–2199.
[40] A. Ahmad, M.H. Razali, M. Mamat, F.S.B. Mehamod, K.A.M. Amin, Adsorption of methyl orange by synthesized and functionalized-CNTs with 3-aminopropyltriethoxysilane loaded TiO_2 nanocomposites, Chemosphere 168 (2017) 474–482.

[41] K. Sui, Y. Li, R. Liu, Y. Zhang, X. Zhao, H. Liang, Y. Xia, Biocomposite fiber of calcium alginate/multi-walled carbon nanotubes with enhanced adsorption properties for ionic dyes, Carbohydr. Polym. 90 (2012) 399–406.
[42] J. Zhang, Q. Zhou, L. Ou, Kinetic, isotherm, and thermodynamic studies of the adsorption of methyl orange from aqueous solution by chitosan/alumina composite, J. Chem. Eng. Data 57 (2) (2012) 412–419.
[43] R. Jiang, Y.Q. Fu, H.Y. Zhu, J. Yao, L. Xiao, Removal of methyl orange from aqueous solutions by magnetic maghemite/chitosan nanocomposite films: adsorption kinetics and equilibrium, J. Appl. Polym. Sci. 125 (2012) E540–E549.
[44] H.Y. Zhu, R. Jiang, L. Xiao, G.M. Zeng, Preparation, characterization, adsorption kinetics and thermodynamics of novel magnetic chitosan enwrapping nanosized γ-Fe_2O_3 and multi-walled carbon nanotubes with enhanced adsorption properties for methyl orange, Bioresour. Technol. 101 (2010) 5063–5069.
[45] H.Y. Zhu, R. Jiang, L. Xiao, Adsorption of an anionic azo dye by chitosan/kaolin/γ-Fe_2O_3 composites, Appl. Clay Sci. 48 (2010) 522–526.
[46] H.Y. Zhu, R. Jiang, L. Xiao, W. Li, A novel magnetically separable γ- Fe_2O_3/crosslinked chitosan adsorbent: preparation, characterization and adsorption application for removal of hazardous azo dye, J. Hazard. Mater. 179 (2010) 251–257.
[47] L. Zeng, M. Xie, Q. Zhang, Y. Kang, X. Guo, H. Xiao, Chitosan/organic rectorite composite for the magnetic uptake of methylene blue and methyl orange, Carbohydr. Polym. 123 (2015) 89–98.
[48] R. Huang, C. Hu, B. Yang, J. Zhao, Zirconium-immobilized bentonite for the removal of methyl orange (MO) from aqueous solutions, Desalin. Water Treat. 57 (2016) 10646–10654.
[49] J. Wang, H. Ma, W. Yuan, W. He, S. Wang, J. You, Synthesis and characterization of an inorganic/organic-modified bentonite and its application in methyl orange water treatment, Desalin. Water Treat. 52 (2014) 7660–7672.
[50] E.H. Mekatel, S. Amokrane, A. Aid, D. Nibou, M. Trari, Adsorption of methyl orange on nanoparticles of a synthetic zeolite NaA/CuO, C. R. Chim. 18 (2015) 336–344.
[51] L. Gan, S. Shang, E. Hu, C.W.M. Yuen, S.X. Jiang, Konjacglucomannan/graphene oxide hydrogel with enhanced dyes adsorption capability for methyl blue and methyl orange, Appl. Surf. Sci. 357 (2015) 866–872.
[52] M. Gao, Q. Ma, Q. Lin, J. Chang, W. Bao, H. Ma, Combined modification of fly ash with $Ca(OH)_2$/Na_2FeO_4 and its adsorption of methyl orange, Appl. Surf. Sci. 359 (2015) 323–330.
[53] S.S. Bayazit, Magnetic multi-wall carbon nanotubes for methyl orange removal from aqueous solutions: equilibrium, kinetic and thermodynamic studies, Sep. Sci. Technol. 49 (2014) 1389–1400.
[54] L. Zeng, M. Xe, Q. Zhang, Y. Kang, X. Guo, H. Xiao, Y. Peng, J. Luo, Chitosan/organic rectorite composite for the magnetic uptake of methylene blue and methyl orange, Carbohydr. Polym. 123 (2015) 89–98.
[55] R. Huang, Q. Liu, J. Huo, B. Yang, Adsorption of methyl orange onto protonated cross-linked chitosan, Arab. J. Chem. 10 (2017) 24–32.
[56] Z.A. AlOthman, M.A. Habila, R. Ali, A.A. Ghafar, M.S.E. Hassouna, Valorization of two waste streams into activated carbon and studying its adsorption kinetics, equilibrium isotherms and thermodynamics for methylene blue removal, Arab. J. Chem. 7 (2014) 1148–1158.